



Research paper

Design, synthesis and biological evaluation of new coumarin-dithiocarbamate hybrids as multifunctional agents for the treatment of Alzheimer's disease

Neng Jiang^{a, b, 1}, Qichun Huang^{b, 1}, Jing Liu^c, Ningsheng Liang^{b, *}, Qing Li^d, Qinghua Li^e, Sai-Sai Xie^{a, **}

^a National Pharmaceutical Engineering Center for Solid Preparation in Chinese Herbal Medicine, Jiangxi University of Traditional Chinese Medicine, Nanchang 330006, PR China

^b Department of Pharmacy, Affiliated Tumor Hospital of Guangxi Medical University, Nanning 530021, Guangxi, PR China

^c School of Pharmacy, Jiangxi University of Traditional Chinese Medicine, Nanchang 330006, PR China

^d Pharmaceutical College, Guangxi Medical University, Shuangyong Road, Nanning 530021, Guangxi, PR China

^e Guangxi Key Laboratory of Brain and Cognitive Neuroscience, Guilin Medical University, 109 North 2nd Huan Cheng Road, Guilin 541004, PR China

ARTICLE INFO

Article history:

Received 24 November 2017

Received in revised form

29 December 2017

Accepted 17 January 2018

Keywords:

Alzheimer's disease

Coumarin

Dithiocarbamate

Cholinesterase

Multifunctional agents

ABSTRACT

A series of new coumarin-dithiocarbamate hybrids were designed, synthesized and evaluated as multifunctional agents for the treatment of Alzheimer's Disease (AD). The biological assays indicated that most of them showed potent inhibition and excellent selectivity towards acetylcholinesterase (AChE), and could inhibit self-induced β -amyloid ($A\beta$) aggregation. Especially, compound **4n** presented the highest ability to inhibit AChE (IC_{50} , 0.027 μ M for hAChE) and good inhibition of $A\beta$ aggregation (40.19% at 25 μ M). Kinetic and molecular modeling studies revealed that **4n** was a mixed-type inhibitor, which could interact simultaneously with the catalytic active site (CAS) and peripheral anionic site (PAS) of AChE. In addition, it also possessed specific metal-chelating ability, good BBB permeability and low toxicity on SH-SY5Y neuroblastoma cells. Moreover, compound **4n** did not exhibit any acute toxicity in mice at doses up to 1000 mg/kg, and could reverse the cognitive dysfunction of scopolamine-induced AD mice. As far as we know, **4n** was the first reported dithiocarbamate derivative with multifunctional activity. Its excellent profiles in vitro and effectivity in vivo highlight this structurally distinct compound as a potential lead compound in the research of innovative multifunctional drugs for AD.

© 2018 Elsevier Masson SAS. All rights reserved.

1. Introduction

Alzheimer's disease (AD), characterized by memory loss, decline in language skills and many other cognitive impairments, is an age-related neurodegenerative disorder and a global public health issue [1,2]. Today, the dementia number is estimated 46 million people worldwide and that is expected to reach 131.5 million by 2050 [3]. Due to the complexity and unidentified etiopathogenesis, many factors are thought to be related to the initiation and development of AD, including deficits of acetylcholine (ACh), amyloid- β ($A\beta$)

peptide deposits, dyshomeostasis of biometals, oxidative stress and hyperphosphorylated tau protein [4].

Among the various pathogenic factors of AD, current clinical treatment of AD has mainly focused on deficits of acetylcholine (ACh). The palliative drugs approved by the FDA consists of four acetylcholinesterase inhibitors (AChEIs), tacrine (now withdrawn the market due to hepatotoxicity), donepezil, rivastigmine and galantamine (Fig. 1a) [5]. Base on cholinergic hypothesis, the decline levels of ACh leads to memory deficits and cognitive impairments, and reducing the ACh metabolism is beneficial to improvement in memory and cognitive dysfunction [6]. There are two types of cholinesterases that can hydrolyze ACh in the central nervous system (CNS), namely acetylcholinesterase (AChE) and butyrylcholinesterase (BuChE) [7]. Although a few studies suggested that BuChE played a significant role in AD pathophysiology, the mechanism of BuChE was not yet completely identified. In

* Corresponding author.

** Corresponding author.

E-mail addresses: Liangn01@163.com (N. Liang), xiesaisainanchang@hotmail.com (S.-S. Xie).

¹ These authors contributed equally.

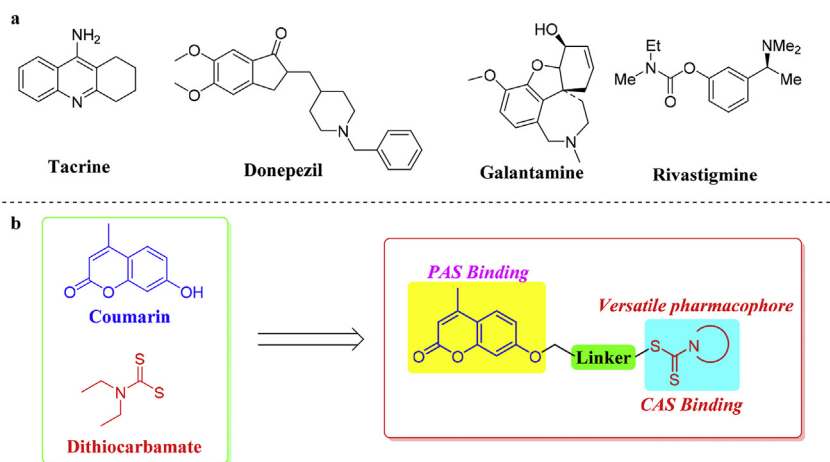


Fig. 1. (a) AChE inhibitors used for the treatment of AD. (b) Design strategy for coumarin-dithiocarbamate hybrids.

addition, BuChE primarily distributes in peripheral system such as plasma, liver and muscle tissues, and accordingly BuChE inhibitor may potentially result in peripheral side effects. For example, tacrine, a dual AChE and BuChE inhibitor, has worst hepatotoxicity and other peripheral adverse reaction [8,9]. Therefore, discovery of effective and selective AChE inhibitors with lower side effects may be more valuable for the treatment of AD. The crystallographic structure of AChE reveals that it has a nearly 20 Å deep narrow gorge which consists of two binding sites: a catalytic active site (CAS) at the bottom of the gorge and a peripheral anionic site (PAS) near the entry of the gorge [10,11]. Research suggest that AChE inhibitors should contain a core ring system that binds to PAS, a basic center that interact with CAS, and a linker, such as, CH₂, –S–, –O–, and CONH(CH₂)_n, etc., between the core ring system and the basic center to fulfil the structural requirements [12].

Another significant hypothesis reveals that Aβ plaques in the brain plays a crucial role in AD pathogenesis. The amyloid precursor protein (APP) is hydrolyzed by α, β, γ-secretase enzymes to produce Aβ peptides that can aggregate into monomers, oligomers and large Aβ plaques [13,14]. These aggregates can initiate pathogenic cascade and ultimately lead to the neuronal loss and dementia [15]. The Aβ peptides have two key isoforms: Aβ₁₋₄₀ and Aβ₁₋₄₂. Aβ₁₋₄₂ shows lower solubility and is more prone to aggregate into fibrils than Aβ₁₋₄₀ [16]. The Aβ plaques generated from Aβ₁₋₄₂ lead to severe neuronal toxicity [17]. Hence, the prevention of Aβ₁₋₄₂ aggregation could serve as a rational strategy for the treatment of AD. Studies also reveal that AChE can facilitate amyloid fibril formation through the interaction with the PAS of AChE, giving stable AChE-Aβ complexes, which are more toxic than single Aβ peptides. Dual-site inhibitors that bind simultaneously to the PAS and CAS of AChE can not only stimulate the cholinergic system, but also inhibit the Aβ aggregation promoted by AChE [18]. Therefore, dual-site inhibitors are thought to be more promising anti-AD drug candidates.

Recently, many studies show that there are excessive bio-metal ions (Cu, Zn, Fe) in the brains of AD patients, which is several-fold higher than that of healthy person [19]. The excessive metal ion is able to interact with Aβ peptides and then accelerate the Aβ aggregates and neurofibrillary tangles, which lead to dysfunction and neuron death [20]. On the other hand, excess of these redox-active metals that interact with Aβ is able to contribute to the production of reactive oxygen species (ROS) and cause the oxidative damage of the central nervous systems (CNS) [21,22]. Hence, modulating these

biometal ions in the brain may be a potential therapeutic method for the AD treatment.

So far, there are only four AChE inhibitors and one N-methyl-D-aspartate receptor antagonist approved by FDA for clinical treatment of AD. Although these drugs can temporarily improve the cognitive and daily function, they cannot mitigate or halt the progression of AD. Due to the complex etiology disease networks, an efficient therapy is more inclined to discover multifunctional drugs that can simultaneously modulate the complex etiology networks. Therefore, many medicinal chemists have made great efforts to develop multifunctional molecules by incorporating several different active structural fragments into one molecule for the treatment of multi-factor neurodegenerative diseases [23,24].

Coumarins, an important group of naturally occurring compounds with small molecular weight, exist in various plant species. Coumarins have attracted increasingly attention in recent years due to a wide of biological activities related to neurological disorders [24–28], such as AChE inhibition, anti-Aβ aggregation and MAO-B inhibition. Our previous studies demonstrated that coumarin was able to bind to the PAS of AChE *via* aromatic π-π stacking interactions [24,29] and therefore could serve as one part of the dual-binding mode of action. On the other hand, dithiocarbamate is a versatile pharmacophore and has been widely used for drug design [30]. However, to our knowledge, there are few reports about the research on dithiocarbamate derivatives against AD. Recently, we found that dithiocarbamate could serve as the other part that bind to the CAS of AChE. Meanwhile, considering the broad activities of dithiocarbamate, we reasoned that compounds containing this group might exert multifunctional activity for the treatment of AD.

Therefore, to further find new dual-acting AChE inhibitors with potential multifunctional activity, in this study, we attempted to connect coumarins (binding to PAS) with the dithiocarbamate moieties (binding to CAS) to design a series of new coumarin-dithiocarbamate hybrids as multifunctional agents (Fig. 1b). All designed compounds were synthesized and evaluated for ChE inhibition and anti-Aβ aggregation. Besides, the outstanding compound was selected for further evaluation including metal chelation, the ability to cross the blood-brain barrier (BBB) *in vitro*, acute toxicity and neuroprotective effects in scopolamine-induced cognitive impairment in mice. Furthermore, kinetic and molecular modeling studies were also carried out to investigate the binding mode of compounds with AChE.

2. Results and discussion

2.1. Chemistry

The synthetic route of the target compounds **4a–q** is illustrated in Scheme 1. Following our reported procedure [31], compound **2** was afforded by condensing resorcinol with ethyl acetoacetate in the presence of a catalytic amount of concentrated sulfuric acid. Then, **2** was reacted with the corresponding α, ω -dibromoalkanes to produce the intermediates **3a–f**. Finally, using a one-pot procedure [32], the target compounds **4a–q** was obtained in good yields by the reaction of **3a–f** with the appropriate secondary amines, carbon disulfide and TEA in DMF.

2.2. In vitro inhibition of ChEs

The inhibitory activities of the test compounds **4a–q** against hAChE and hBuChE were determined according to the spectrophotometric method described by Ellman et al. [33]. For comparison purpose, the well-known cholinesterase inhibitors, donepezil and tacrine, were used as reference compounds. The experimental results were presented as IC_{50} (μ M), or for poorly active compounds, as the percentage of inhibition at 10μ M. All these results are summarized in Table 1.

From the table, it can be seen that the terminal amine groups connected with the dithiocarbamate moiety play an important role in AChE inhibition. Compounds **4c** and **4d** with cyclic amine groups (pyrrolidinyl and piperidinyl) in side chains showed more potent activity than compounds **4a** and **4b** containing an alkyl amine group (dimethylamino and diethylamino). And piperidinyl group seemed more beneficial for AChE inhibition than pyrrolidinyl group since compound **4d** ($IC_{50} = 0.47 \pm 0.23 \mu$ M) exhibited nearly 2-fold more potent activity than compound **4c** ($IC_{50} = 0.89 \pm 0.11 \mu$ M). However, introducing another piperidinyl substituent to 4-position of piperidinyl moiety afforded compound **4k**, which gave rise to a decrease in AChE inhibition ($IC_{50} = 1.16 \pm 0.12 \mu$ M). Morpholinyl, 4-hydroxypiperidine and diethanolamino groups were not beneficial for AChE inhibition, as compounds **4e–g** showed the inhibitory activity, which was less than 50% at 10μ M. This result suggested that the oxygen atom at the terminal moiety was not tolerated for AChE inhibition. Unlike previous reports that indicated 4-substituted piperazine could enhance the inhibitory activity for AChE [34,35], the present compounds **4h–j** and **4l** did not show improved activity compared to compound **4d**. With exception of compound **4i**, most of the compounds (**4h**, **4j** and **4l**) containing

piperazine moiety only presented very weak inhibition for AChE. However, it is interesting to note that the substitutes at 4-position of piperazine moiety were very sensitive to inhibitory activity. Compound **4i** ($IC_{50} = 1.99 \pm 0.06 \mu$ M) bearing an isopropyl group exerted much higher activity than compounds **4h** and **4j** possessing methyl (36.84% inhibition) and cyclopropyl (18.69% inhibition) substituents. Taken together, the above results indicated that piperidinyl group was the optimal substitution pattern for AChE inhibition, and compound **4d** possessing relatively high activity was selected for further optimization.

After lengthening the linker length between coumarin and dithiocarbamate moiety in compound **4d** from two to eight carbon atoms, the new obtained compound **4n** with a four-carbon atom linker exhibited the best inhibition for AChE in this series. It showed the IC_{50} value of 0.027μ M, which was 1.5-fold more potent than that of donepezil ($IC_{50} = 0.041 \pm 0.001 \mu$ M).

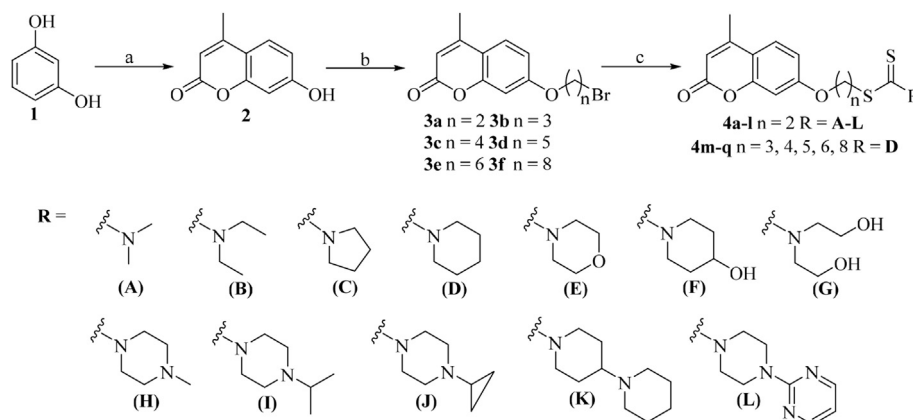
Finally, all compounds displayed inactive or very weak activity for BuChE. This result demonstrated that most of the present compounds were selective inhibitors to AChE. In view of BuChE was mainly localized in the peripheral tissues and very small amount was present in the brain region [36]. Therefore, these compounds would result in lesser degree of associated side effects and might be more beneficial for AD treatment.

2.3. Kinetic studies for the inhibition of AChE

In order to investigate the inhibition mechanism of the present compounds for AChE, the most potent inhibitor, compound **4n**, was selected for kinetic study. Analysis of the Lineweaver-Burk reciprocal plot ($1/V$ vs $1/S$) showed both increasing slopes and intercepts at increasing concentration of the inhibitor (Fig. 2a). This pattern indicated a mixed-type inhibition and therefore revealed that compound **4n** might be able to bind to the catalytic active site (CAS) as well as peripheral anionic site (PAS) of AChE. Replots of the slope versus concentration of **4n** gave an estimate of competitive inhibition constant, K_i , of 37.14 nM (Fig. 2b).

2.4. Molecular modeling study of AChE inhibition

In order to explore more information about the binding interactions between compound **4n** and AChE, a molecular modeling study was carried out using the Molecular Operating Environment (MOE 2008.10) software package. The X-ray crystal structure of the recombinant human acetylcholinesterase in complex with donepezil (hAChE, PDB code 4EY7) was applied to establish the starting



Scheme 1. Synthesis of compounds **4a–q**. Reagents and conditions: (a) Ethyl acetoacetate, conc. H_2SO_4 (cat.), 1,4-dioxane, $60^\circ C$, 4 h; (b) $Br(CH_2)_nBr$, anhydrous K_2CO_3 , acetone, reflux, 4 h; (c) appropriate secondary amines, CS_2 , TEA, DMF, r.t., 12 h.

Table 1
Inhibition of hAChE, hBuChE and self-induced A β_{1-42} aggregation by compounds **4a–q**.

Compd.	n	R	AChE		BuChE Inhibition (%) ^b	A β aggregation inhibition (%) ^d
			IC ₅₀ (μ M)/inhibition (%) ^a			
4a	2	A	10.59 \pm 1.34		n.a. ^c	24.55 \pm 1.25
4b	2	B	1.94 \pm 0.56		10.89 \pm 1.58	29.08 \pm 0.98
4c	2	C	0.89 \pm 0.11		n.a. ^c	33.22 \pm 1.67
4d	2	D	0.47 \pm 0.23		37.24 \pm 5.13	37.88 \pm 2.49
4e	2	E	10.99 \pm 1.26%		n.a. ^c	20.02 \pm 0.99
4f	2	F	n.a. ^c		n.a. ^c	17.83 \pm 1.02
4g	2	G	34.49 \pm 3.08%		n.a. ^c	16.12 \pm 0.07
4h	2	H	36.84 \pm 2.51%		n.a. ^c	34.02 \pm 2.15
4i	2	I	1.99 \pm 0.06		28.10 \pm 2.82	35.44 \pm 1.33
4j	2	J	18.69 \pm 2.00%		n.a. ^c	34.07 \pm 2.55
4k	2	K	1.16 \pm 0.12		24.27 \pm 2.06	43.53 \pm 3.11
4l	2	L	12.33 \pm 1.59%		n.a. ^c	27.39 \pm 0.95
4m	3	D	0.29 \pm 0.07		31.24 \pm 3.12	37.03 \pm 1.65
4n	4	D	0.027 \pm 0.002		15.29 \pm 1.95	40.19 \pm 2.39
4o	5	D	0.21 \pm 0.03		10.10 \pm 1.02	40.03 \pm 1.05
4p	6	D	0.61 \pm 0.08		6.21 \pm 0.99	33.86 \pm 2.01
4q	8	D	n.a. ^c		n.a. ^c	10.02 \pm 0.07
Donepezil	–	–	0.041 \pm 0.001		IC ₅₀ = 4.22 \pm 0.20 μ M	n.a. ^e
Tacrine	–	–	0.43 \pm 0.02		IC ₅₀ = 0.021 \pm 0.001 μ M	–
Curcumin	–	–	–		–	39.62 \pm 3.35

^a The 50% inhibitory concentration of human AChE or percent inhibition with inhibitor at 10 μ M (means \pm SD of three experiments).

^b The percent inhibition of human BuChE with inhibitor at 10 μ M (means \pm SD of three experiments).

^c n. a. = no active. Compounds defined “no active” means that percent inhibition is less than 5.0% at a concentration of 10 μ M in the assay conditions.

^d Inhibition of self-induced A β_{1-42} aggregation by tested inhibitors at 25 μ M.

^e n.a. = no active. Compounds defined “no active” means that percent inhibition was less than 5% at 25 μ M.

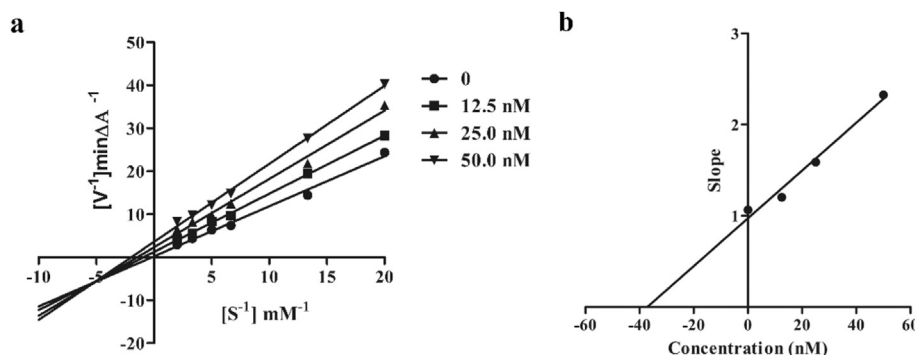


Fig. 2. (a) Kinetic study on the mechanism of AChE inhibition by compound **4n**. Overlaid Lineweaver–Burk reciprocal plots of AChE initial velocity at increasing substrate concentration (0.05–0.50 mM) in the absence of inhibitor and in the presence of different concentrations of **4n** are shown. (b) The plot of the slopes of the Lineweaver–Burk plots versus inhibitor concentration.

model of AChE. As shown in Fig. 3, the coumarin moiety was bound to the PAS of the enzyme, establishing a π - π stacking interaction between its phenyl ring and the indole ring of Trp 286 (3.92 Å). Besides, the carbonyl oxygen of coumarin moiety also formed a hydrogen bond with Ser 293 in PAS (2.97 Å). The piperidinyldithiocarbamate moiety of compound **4n** was located into the CAS and showed a hydrophobic interaction with residues Gly 448, Trp 86, Tyr337 and Gly 121. In addition, the side chain between coumarin and dithiocarbamate moiety folded in a conformation in the gorge that allowed it to interact with Phe 338, Tyr 341, Tyr 124 and Phe 295 via hydrophobic interactions. Taken together, all these results indicated that compound **4n** occupied the entire enzymatic CAS, the mid-gorge site and the PAS, and could bind simultaneously to both the PAS and CAS.

2.5. Inhibition of self-induced A β_{1-42} aggregation

All compounds tested for ChEs inhibition were also evaluated by a thioflavin T-based fluorometric assay for their ability to inhibit

self-induced A β_{1-42} aggregation [37]. Curcumin, a known active natural product for inhibition of A β_{1-42} self-aggregation, was used as reference compound. From the results summarized in Table 1 and Fig. 4, it can be seen that most of the compounds show moderate to good potencies (10.02–43.53% at 25 μ M) compared with curcumin (39.62% at 25 μ M). Compounds **4k**, **4n** and **4o** (43.53%, 40.19%, and 40.03% at 25 μ M, respectively) were the best inhibitors in this series, which showed the percent inhibition better than that of curcumin. Unlike the AChE inhibition, compounds with different terminal secondary amines and varied linker length did not give a clear trend in A β_{1-42} aggregation inhibition. However, it is interesting to note that 4-piperidinopiperidine group seemed more beneficial for inhibitory activity, as compound **4k** gave the highest inhibitory activity for A β_{1-42} aggregation. Given all above results, compound **4n** with the most potent inhibitory activity for hAChE and the second highest inhibition potency for A β_{1-42} aggregation was selected as promising compound for further study.

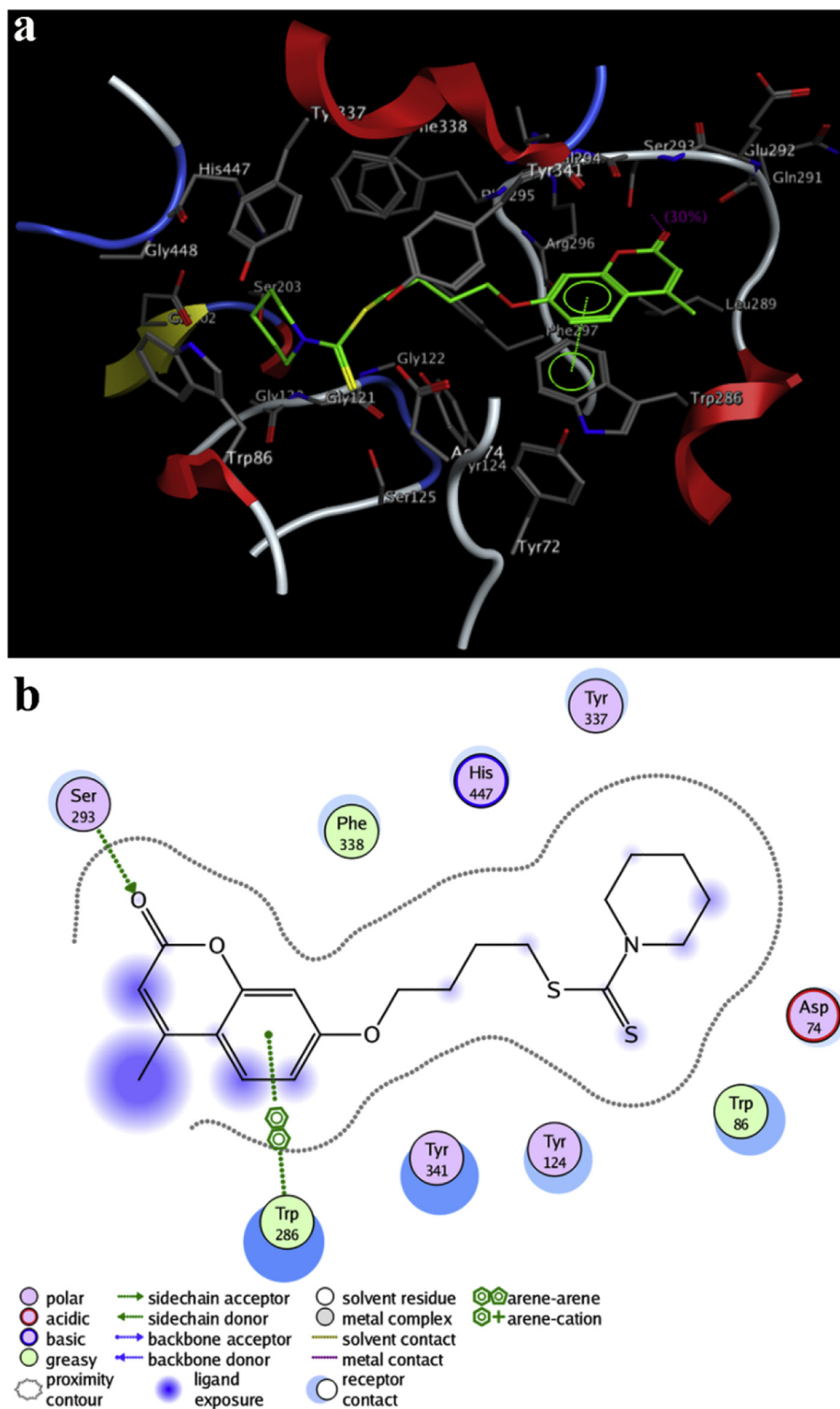


Fig. 3. (a) 3D docking model of compound **4n** with hAChE. Atom colours: green—carbon atoms of **4n**, grey—carbon atoms of residues of hAChE, dark blue—nitrogen atoms, red—oxygen atoms, yellow—sulfur atom. The dashed lines represent the interactions between the protein and the ligand. (b) 2D schematic diagram of docking model of compound **4n** with hAChE. The figure was prepared using the ligand interactions application in MOE. (For interpretation of the references to colour in this figure legend, the reader is referred to the Web version of this article.)

2.6. Metal-chelating studies

The ability of compound **4n** to chelate biometals, such as Cu^{2+} , Zn^{2+} , Fe^{2+} and Fe^{3+} was evaluated by a UV–vis spectroscopy assay [38]. As shown in Fig. 5a, Fe^{3+} caused an obvious absorption

strength enhancement, while Cu^{2+} and Fe^{2+} had relatively weak effects on the absorbance at the same concentration and conditions. However, when Zn^{2+} were added, no significant change was observed for UV–vis spectra. These results indicated that compound **4n** could selectively chelate the metals and was more

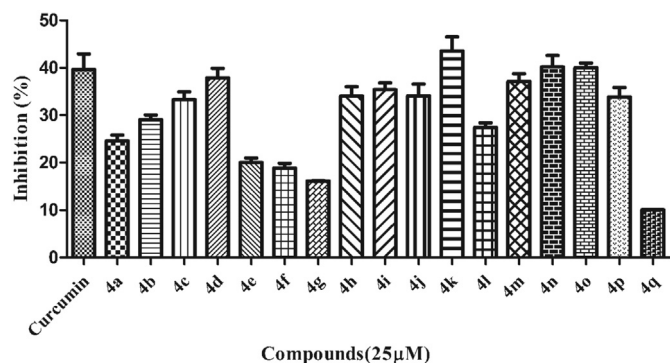


Fig. 4. Inhibition of self-induced $A\beta_{1-42}$ aggregation by compounds **4a–q** comparing with that of curcumin. The thioflavin-T fluorescence method was used and the measurements were carried out in the presence of $25 \mu\text{M}$ test compound. The mean \pm SD values from three independent experiments were shown.

sensitive to chelate Fe^{3+} .

To further understand the interactions between compound **4n** and Fe^{3+} , Job's method was performed to determine the stoichiometry of the **4n**- Fe^{3+} complex [39]. After keeping total concentration of compound and Fe^{3+} at $50 \mu\text{M}$ and changing the molar ratio of Fe^{3+} from 0.1 to 0.9, the absorbance of Job's plot curve got to maximum when the molar fraction of Fe^{3+} was 0.5, which revealed a 1:1 stoichiometry for the complex (Fig. 5b). Moreover, the association constant (K_a) of the complex was also calculated using the Benesi-Hildebrand equation [39,40], and the value of K_a was $1.69 \times 10^3 \text{ M}^{-1}$, suggesting that compound **4n** could moderately chelate Fe^{3+} .

2.7. SH-SY5Y neuroblastoma cell toxicity

To investigate the cytotoxicity of compound **4n**, the human neuroblastoma cell line SH-SY5Y were exposed to **4n** at different concentrations (12.5, 25, 50 and $100 \mu\text{M}$) for 24 h, and the cell viability was determined by the 3-(4, 5-dimethylthiazol-2-yl)-2, 5-diphenyltetrazolium (MTT) assay [41]. The results indicated that compound **4n** showed negligible cell death up to the concentration of $50 \mu\text{M}$ (12.5 μM : $99.2 \pm 1.4\%$; 25 μM : $101.1 \pm 10.3\%$; 50 μM : $90.1 \pm 2.4\%$). After increasing the concentration to $100 \mu\text{M}$, compound **4n** showed a decrease of cell viability ($100 \mu\text{M}$: $80.3 \pm 1.5\%$).

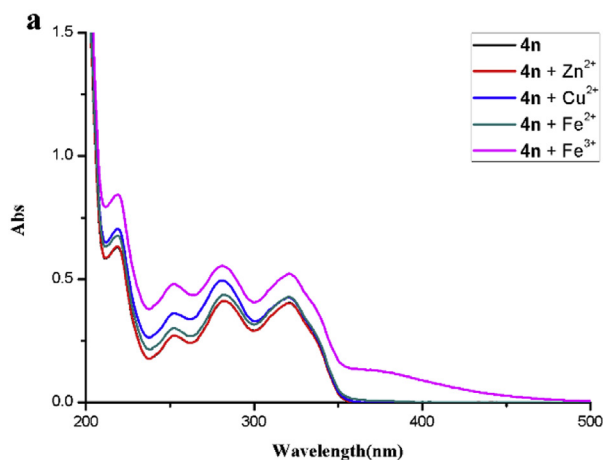


Table 2
Permeability P_e ($\times 10^6 \text{ cm/s}$) in the PAMPA-BBB assay for 10 commercial drugs in the experiment validation.

Commercial drugs	Bibliography ^a	Experiment ^b
Testosterone	17.0	24.0 ± 0.9
Verapamil	16.0	19.8 ± 0.8
Imipramine	13.0	15.1 ± 1.5
Progesterone	9.3	16.2 ± 0.6
Clonidine	5.3	5.1 ± 0.2
Corticosterone	5.1	6.3 ± 0.5
Piroxicam	2.5	4.5 ± 0.3
Caffeine	1.3	3.3 ± 0.1
Lomefloxacin	1.1	2.9 ± 0.2
Ofloxacin	0.8	1.1 ± 0.1

^a Taken from Ref. [42].

^b Experimental data are the mean \pm SD of 3 independent experiments, using PBS: EtOH (70:30) as solvent.

Therefore, these results proved that compound **4n** was low cytotoxicity to SH-SY5Y cells.

2.8. In vitro blood–brain barrier permeation assay

Blood-brain barrier (BBB) permeability is a first requirement for successful CNS drugs. Therefore, to determine whether the selected compound **4n** could be able to penetrate into the brain, the parallel artificial membrane permeation assay for blood-brain barrier (PAMPA-BBB) was performed [42]. After comparing experimental permeabilities of 10 commercial drugs with reported values (Table 2), a plot of experiment data versus the bibliographic values gave a good linear correlation: $P_e(\text{exp.}) = 1.2653 P_e(\text{bibl.}) + 0.7955$ ($R^2 = 0.9483$) (Fig. 6). From this equation and taking into account the limits established by Di et al. for BBB permeation, we classified compounds as follows:

- 'CNS+' (high BBB permeation predicted): P_e (10^{-6} cm/s) > 5.86
- 'CNS-' (low BBB permeation predicted): P_e (10^{-6} cm/s) < 3.33
- 'CNS+/-' (uncertain BBB permeation): $3.33 < P_e$ (10^{-6} cm/s) < 5.86

According to the measured permeability, compound **4n** showed a P_e value of $9.21 \times 10^{-6} \text{ cm/s}$, which indicated that it could penetrate the BBB and reach the biological targets in the CNS.

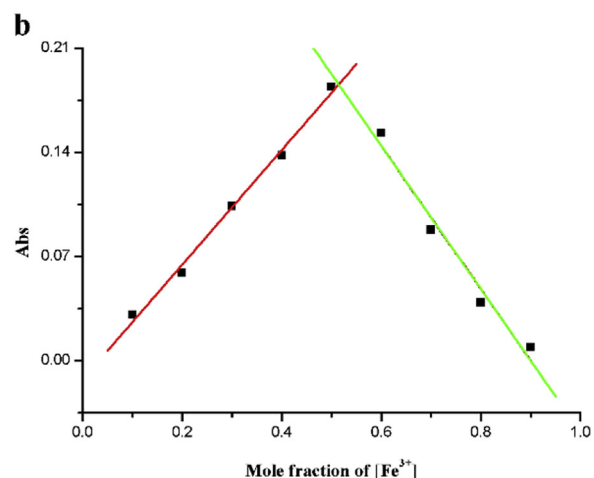


Fig. 5. (a) The UV-vis absorption spectra of compound **4n** ($25 \mu\text{M}$) alone or in the presence of $50 \mu\text{M}$ of CuCl_2 , ZnCl_2 , FeSO_4 and $\text{Fe}_2(\text{SO}_4)_3$ in MeOH solution. (b) Job's plot of compound **4n** with Fe^{3+} in MeOH solution. Total concentration was kept constant at $50 \mu\text{M}$ and the absorbance at 373 nm was used.

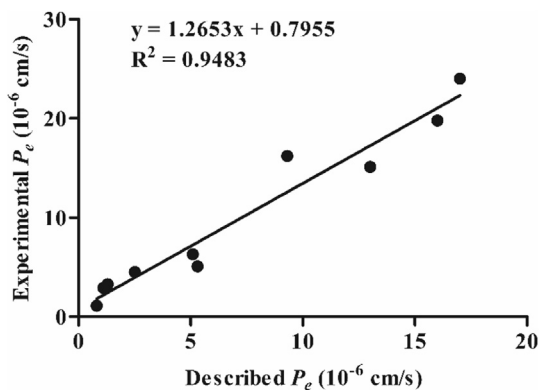


Fig. 6. Lineal correlation between experimental and reported permeability of commercial drugs using the PAMPA-BBB assay. P_e (exp.) = 1.2653 P_e (bibl.) + 0.7955 ($R^2 = 0.9483$).

2.9. Acute toxicity test

The acute toxicity profile is an important criterion in the development of new drugs. Therefore, the most potent compound **4n** was selected for evaluation in KM mice according to the reported method [43,44]. After administration of the compound (1000 mg/kg), mice were monitored continuously for the first 4 h for any abnormal behavior and mortality changes, intermittently for the next 24 h, and occasionally thereafter for 14 days to monitor the onset of any delayed effects. During the experimental period, no acute toxicity, such as significant abnormal changes in water or food consumption, or body weight reduction or mortality, was observed. Furthermore, all mice were sacrificed on the 14th day after drug administration and macroscopically examined for possible damage to the heart, liver and kidneys. The results indicated that compound **4n** did not develop any acute toxicity and well tolerated at doses up to 1000 mg/kg.

2.10. In vivo assay

As compound **4n** showed excellent results on the above studies, it was necessary to determine whether it could improve memory impairment in vivo. After establishing the classical scopolamine-induced cognitive deficit mouse model, a step-down passive avoidance test was performed to evaluate the effect of compounds **4n** on cognitive improvement [45,46], and donepezil was used as positive control. It can be seen from Fig. 7 that the model group exhibit much shorter latency and more number of errors than the

control group ($^{##}p < .01$). Treatment with compound **4n** (20.6, 10.3 and 5.2 mg/kg) could increase the latency and reduce the number of errors in a dose-dependent manner. The high dose group of compound **4n** (20.6 mg/kg) presented a longer latency (192 s) and less number of errors (1.75) than donepezil group (181 s; 2.00). Meanwhile, the medium dose group (10.3 mg/kg) also showed the comparable effects (182 s; 1.89) to donepezil group. However, for the low dose group (5.2 mg/kg), it didn't exhibit significant difference compared with model group, but the latency (151 s) and number of errors (2.5) were largely improved. All in all, these results demonstrated that compound **4n** could cross the blood-brain barrier and reverse cognitive deficit by increasing brain cholinergic activity due to the inhibition of AChE.

3. Conclusion

To develop effective drugs for the treatment of AD, a series of new multifunctional hybrids **4a-q** by connecting coumarin with dithiocarbamate moiety were designed, synthesized and evaluated. The results indicated that most of these compounds showed potent AChE inhibitory activity and high selectivity for AChE over BuChE. Compound **4n** ($IC_{50} = 0.027 \mu M$) showed the best inhibitory activity to hAChE, which was 1.5-fold more potent than that of donepezil. Kinetic and molecular modeling study suggested that compound **4n** was a mix-typed inhibitor, which could bind simultaneously to PAS and CAS of AChE. In addition, compound **4n** could effectively inhibit A β aggregation (40.19% at 25 μM) and selectively chelate Fe^{3+} ion. It also showed good ability to penetrate the BBB in vitro and exhibited low toxicity to SH-SY5Y cells. More importantly, our in vivo study proved that **4n** did not display acute toxicity in mice at doses up to 1000 mg/kg, and mice treated with **4n** (20.6 and 10.3 mg/kg, p.o.) could significantly prolong the latency and reduce number of errors in the step-down passive avoidance test. To the best of our knowledge, compound **4n** was the first reported compound containing a dithiocarbamate moiety, which have multifunctional activity. Such excellent properties rendered compound **4n** a potential lead compound deserved for further study, and dithiocarbamate moiety could be used as a new scaffold for designing innovative multifunctional drugs for the treatment of AD.

4. Experimental section

4.1. Chemistry

All chemical reagents used in synthesis were obtained from Sinopharm Chemical Reagent Co., Ltd. (China). The reactions were monitored by TLC on glass-packed precoated silica gel GF₂₅₄

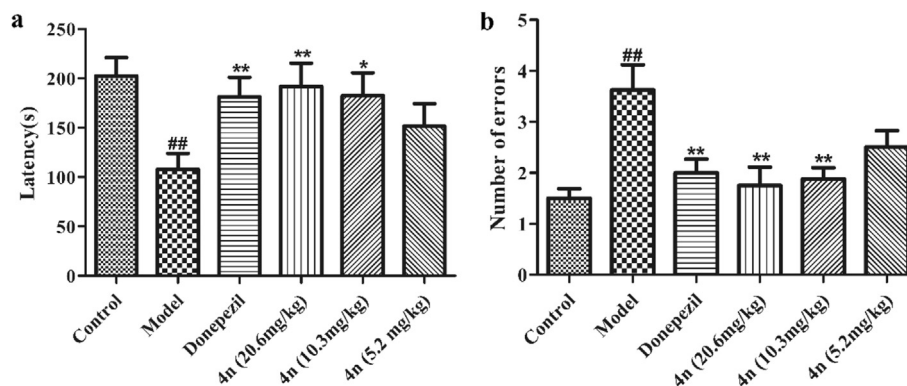


Fig. 7. Effects of compound **4n** on the (a) latency (s) and (b) number of errors in the step-down test by the scopolamine-induced cognitive impairment. The data shown are mean \pm SEM ($n = 8$). $^{##}P < .01$ vs. control group, $^*P < .05$, $^{**}P < .01$ vs. model group.

(Qingdao Haiyang Chemical Plant, Qingdao, China) plates. Column chromatography was performed on silica gel (90–150 μm ; Qingdao Marine Chemical Inc.). Melting point was measured on an XT-4 micromelting point instrument and uncorrected. ^1H NMR spectra (600 MHz) and ^{13}C NMR spectra (151 MHz) were recorded on a Bruker ACF-600 spectrometer at 25 °C. Chemical shifts are reported in ppm (δ) using the TMS as internal standard, and the coupling constants are reported in hertz (Hz). The purity of all compounds for biological evaluation was confirmed to >95% by analytical HPLC conducted on an Agilent 1200 HPLC System. Mass spectra were carried out on a Thermo Scientific LCQ Fleet mass spectrometer (ESI-MS) and an AB Sciex Triple TOF 5600 spectrometer (HR-ESI-MS), respectively.

4.2. 7-Hydroxy-4-methyl-2H-chromen-2-one (**2**)

To an ice-cold solution of resorcinol (5.5 g, 50 mmol) in dioxane, conc. H_2SO_4 (2 mL) was added dropwise under 25 °C. After the addition of concentrated sulfuric acid, ethylacetoacetate (7 mL) was added and the mixture was heated to 60 °C for 4 h. Then, the mixture was poured into cold water and the precipitate was filtered and dried under reduced pressure. The resulting mixture was recrystallized from methanol to give **2** as white needle crystals, yield 91%; m.p. 186–187 °C; ^1H NMR (600 MHz, acetone- d_6) δ 7.61 (1H, d, $J = 9.0$ Hz), 6.85 (1H, dd, $J = 9.0, 2.5$ Hz), 6.75 (1H, d, $J = 2.5$ Hz), 6.09 (1H, s), 2.40 (3H, s). ESI-MS m/z : 175.0 $[\text{M}-\text{H}]^-$.

4.3. General procedure for the preparation of compounds **3a-f**

A mixture of **2** (5.0 mmol) with suitable α, ω -dibromoalkanes (50 mmol) and anhydrous K_2CO_3 (1.4 g, 10 mmol) in acetone (15 mL) was refluxed under stirring for 4 h. After cooling, the reaction mixture was filtered, and the filtrate was evaporated under reduced pressure. The obtained residue was purified by silica gel chromatography with PE/EA (15:1) as eluent to give compounds **3a-f** as white solid.

4.3.1. 7-(2-bromoethoxy)-4-methyl-2H-chromen-2-one (**3a**)

Yield 86%; m.p. 104–105 °C; ^1H NMR (600 MHz, CDCl_3) δ 7.53 (d, $J = 8.8$ Hz, 1H), 6.91 (dd, $J = 8.8, 2.5$ Hz, 1H), 6.83 (d, $J = 2.5$ Hz, 1H), 6.17 (s, 1H), 4.37 (t, $J = 6.1$ Hz, 2H), 3.70 (t, $J = 6.1$ Hz, 2H), 2.40 (s, 3H); ESI-MS m/z : 283.1 $[\text{M}+\text{H}]^+$.

4.3.2. 7-(3-bromopropoxy)-4-methyl-2H-chromen-2-one (**3b**)

Yield 92%; m.p. 82–83 °C; ^1H NMR (600 MHz, CDCl_3) δ 7.51 (d, $J = 8.8$ Hz, 1H), 6.88 (d, $J = 8.8$ Hz, 1H), 6.84 (d, $J = 1.0$ Hz, 1H), 6.15 (s, 1H), 4.19 (t, $J = 5.8$ Hz, 2H), 3.63 (t, $J = 6.3$ Hz, 2H), 2.40 (s, 3H), 2.39–2.35 (m, 2H); ESI-MS m/z : 297.1 $[\text{M}+\text{H}]^+$.

4.3.3. 7-(4-bromobutoxy)-4-methyl-2H-chromen-2-one (**3c**)

Yield 87%; m.p. 58–60 °C; ^1H NMR (600 MHz, CDCl_3) δ 7.52 (d, $J = 8.8$ Hz, 1H), 6.86 (dd, $J = 8.8, 2.5$ Hz, 1H), 6.80 (d, $J = 2.5$ Hz, 1H), 6.14 (s, 1H), 4.07 (t, $J = 6.1$ Hz, 2H), 3.51 (t, $J = 6.6$ Hz, 2H), 2.40 (s, 3H), 2.16–2.05 (m, 2H), 2.03–1.95 (m, 2H); ESI-MS m/z : 311.1 $[\text{M}+\text{H}]^+$.

4.3.4. 7-((5-bromopentyl)oxy)-4-methyl-2H-chromen-2-one (**3d**)

Yield 90%; m.p. 59–60 °C; ^1H NMR (600 MHz, CDCl_3) δ 7.48 (d, $J = 8.8$ Hz, 1H), 6.84 (dd, $J = 8.8, 2.5$ Hz, 1H), 6.79 (d, $J = 2.5$ Hz, 1H), 6.12 (s, 1H), 4.04 (t, $J = 6.1$ Hz, 2H), 3.45 (t, $J = 6.1$ Hz, 2H), 2.41 (s, 3H), 1.94 (br s, 2H), 1.85 (br s, 2H), 1.66 (br s, 2H); ESI-MS m/z : 325.2 $[\text{M}+\text{H}]^+$.

4.3.5. 7-((6-bromohexyl)oxy)-4-methyl-2H-chromen-2-one (**3e**)

Yield 82%; m.p. 58–59 °C; ^1H NMR (600 MHz, CDCl_3) δ 7.50 (d,

$J = 8.8$ Hz, 1H), 6.86 (d, $J = 8.8, 2.0$ Hz, 1H), 6.81 (d, $J = 2.0$ Hz, 1H), 6.14 (s, 1H), 4.03 (t, $J = 6.3$ Hz, 2H), 3.45 (t, $J = 7.2$ Hz, 2H), 2.41 (s, 3H), 1.92 (br s, 2H), 1.85 (br s, 2H), 1.54 (br s, 4H); ESI-MS m/z : 339.1 $[\text{M}+\text{H}]^+$.

4.3.6. 7-((8-bromooctyl)oxy)-4-methyl-2H-chromen-2-one (**3f**)

Yield 85%; m.p. 49–50 °C; ^1H NMR (600 MHz, CDCl_3) δ 7.49 (d, $J = 8.8$ Hz, 1H), 6.86 (d, $J = 9.8$ Hz, 1H), 6.80 (d, $J = 2.5$ Hz, 1H), 6.13 (s, 1H), 4.02 (t, $J = 5.8$ Hz, 2H), 3.42 (t, $J = 6.3$ Hz, 2H), 2.41 (s, 3H), 1.87 (br s, 2H), 1.82 (br s, 2H), 1.48 (br s, 4H), 1.38 (br s, 4H); ESI-MS m/z : 367.2 $[\text{M}+\text{H}]^+$.

4.4. General procedure for the preparation of compounds **4a-q**

CS_2 (99 mg, 1.3 mmol) was added dropwise to the mixture of the secondary amine (1.2 mmol) and TEA (131 mg, 1.3 mmol) in DMF (2 mL). After stirring for 5 min, a solution of the corresponding coumarin derivatives **3a-f** (1.2 mmol) in DMF (3 mL) was added. Then, the reaction mixture was stirred at room temperature for 12 h. When the reaction was completed, water (20 mL) was added and the mixture was extracted with ethyl acetate (10 mL \times 3), the combined organic phase was washed with water (15 mL \times 3), dried over anhydrous Na_2SO_4 and concentrated under vacuum to afford the crude product. The crude product was purified by silica gel chromatography with PE/EA (10:1) as eluent to obtain the target compounds **4a-q**.

4.4.1. 2-((4-Methyl-2-oxo-2H-chromen-7-yl)oxy)ethyl dimethylcarbamodithioate (**4a**)

Yield 85%; yellow solid; m.p. 111–112 °C; ^1H NMR (600 MHz, CDCl_3) δ 7.52 (d, $J = 8.8$ Hz, 1H), 6.93 (dd, $J = 8.8, 2.4$ Hz, 1H), 6.88 (d, $J = 2.4$ Hz, 1H), 6.16 (s, 1H), 4.33 (t, $J = 6.3$ Hz, 2H), 3.78 (t, $J = 6.3$ Hz, 2H), 3.60 (s, 3H), 3.43 (s, 3H), 2.42 (s, 3H). ^{13}C NMR (151 MHz, CDCl_3) δ 196.06, 161.59, 161.37, 155.28, 152.46, 125.30, 113.54, 112.33, 112.17, 102.06, 66.92, 45.68, 41.48, 35.92, 18.64. HRMS: calcd for $\text{C}_{15}\text{H}_{18}\text{NO}_3\text{S}_2$ $[\text{M} + \text{H}]^+$ 324.0723, found 324.0760.

4.4.2. 2-((4-Methyl-2-oxo-2H-chromen-7-yl)oxy)ethyl diethylcarbamodithioate (**4b**)

Yield 82%; white solid; m.p. 126–128 °C; ^1H NMR (600 MHz, CDCl_3) δ 7.54 (d, $J = 8.8$ Hz, 1H), 6.91 (dd, $J = 8.8, 2.4$ Hz, 1H), 6.84 (d, $J = 2.4$ Hz, 1H), 6.18 (s, 1H), 4.07 (t, $J = 6.0$ Hz, 2H), 3.84–3.74 (m, 4H), 3.70 (t, $J = 6.1$ Hz, 2H), 2.43 (s, 3H), 1.38–1.21 (m, 6H). ^{13}C NMR (151 MHz, CDCl_3) δ 194.37, 161.59, 161.02, 155.21, 152.46, 125.76, 113.85, 112.34, 112.14, 102.08, 67.05, 49.87, 46.89, 35.92, 18.70, 12.53, 12.56. HRMS: calcd for $\text{C}_{17}\text{H}_{22}\text{NO}_3\text{S}_2$ $[\text{M} + \text{H}]^+$ 352.1036, found 352.1053.

4.4.3. 2-((4-Methyl-2-oxo-2H-chromen-7-yl)oxy)ethyl pyrrolidine-1-carbodithioate (**4c**)

Yield 87%; yellow solid; m.p. 149–151 °C; ^1H NMR (600 MHz, CDCl_3) δ 7.51 (d, $J = 9.0$ Hz, 1H), 6.93 (dd, $J = 9.0, 2.4$ Hz, 1H), 6.86 (d, $J = 2.4$ Hz, 1H), 6.14 (s, 1H), 4.31 (t, $J = 6.6$ Hz, 2H), 3.95 (t, $J = 6.6$ Hz, 2H), 3.77 (t, $J = 6.6$ Hz, 2H), 3.69 (t, $J = 7.2$ Hz, 2H), 2.40 (s, 3H), 2.10–2.09 (m, 2H), 2.01–1.99 (m, 2H). ^{13}C NMR (151 MHz, CDCl_3) δ 191.56, 161.57, 161.29, 155.20, 152.47, 125.58, 113.86, 112.32, 112.14, 102.07, 67.07, 55.31, 50.73, 34.88, 26.08, 24.30, 18.69. HRMS: calcd for $\text{C}_{17}\text{H}_{20}\text{NO}_3\text{S}_2$ $[\text{M} + \text{H}]^+$ 350.0879, found 350.0904.

4.4.4. 2-((4-Methyl-2-oxo-2H-chromen-7-yl)oxy)ethyl piperidine-1-carbodithioate (**4d**)

Yield 84%; white solid; m.p. 78–79 °C; ^1H NMR (600 MHz, CDCl_3) δ 7.53 (d, $J = 8.8$ Hz, 1H), 6.93 (dd, $J = 8.8, 2.5$ Hz, 1H), 6.88 (d, $J = 2.5$ Hz, 1H), 6.16 (s, 1H), 4.33 (t, $J = 6.3$ Hz, 2H), 3.93 (br s, 2H), 3.81–3.79 (m, 2H), 3.71–3.68 (m, 2H), 2.42 (s, 3H), 1.74 (br s, 6H).

^{13}C NMR (151 MHz, CDCl_3) δ 194.36, 161.61, 161.02, 155.21, 152.46, 125.75, 113.85, 112.56, 112.13, 102.06, 67.11, 53.36, 51.44, 35.47, 28.47, 24.22, 18.69. HRMS: calcd for $\text{C}_{18}\text{H}_{22}\text{NO}_3\text{S}_2$ [$\text{M} + \text{H}$] $^+$ 364.1036, found 364.1062.

4.4.5. 2-((4-methyl-2-oxo-2H-chromen-7-yl)oxy)ethyl morpholine-4-carbodithioate (4e)

Yield 81%, white solid; m.p. 138–139 °C; ^1H NMR (600 MHz, CDCl_3) δ 7.51 (d, $J = 8.4$ Hz, 1H), 6.91 (dd, $J = 9.0, 1.8$, 1H), 6.88 (d, $J = 1.8$ Hz, 1H), 6.14 (s, 1H), 4.37 (br s, 2H), 4.32 (t, $J = 6.2$ Hz, 2H), 3.98 (br s, 2H), 3.81 (t, $J = 6.6$ Hz, 2H), 3.78 (br s, 4H), 2.40 (s, 3H). ^{13}C NMR (151 MHz, CDCl_3) δ 196.37, 161.47, 161.23, 155.20, 152.43, 125.61, 113.92, 112.32, 112.20, 101.99, 66.83, 66.35, 66.10, 51.61, 50.49, 35.38, 18.69. HRMS: calcd for $\text{C}_{17}\text{H}_{20}\text{NO}_4\text{S}_2$ [$\text{M} + \text{H}$] $^+$ 366.0828, found 366.0865.

4.4.6. 2-((4-Methyl-2-oxo-2H-chromen-7-yl)oxy)ethyl 4-hydroxypiperidine-1-carbo dithioate (4f)

Yield 83%; yellow solid; m.p. 160–162 °C; ^1H NMR (600 MHz, CDCl_3) δ 7.52 (d, $J = 8.8$ Hz, 1H), 6.93 (dd, $J = 8.8, 2.4$ Hz, 1H), 6.88 (d, $J = 2.4$ Hz, 1H), 6.16 (s, 1H), 4.62 (s, 1H), 4.35 (t, $J = 6.3$ Hz, 2H), 4.25–4.21 (m, 2H), 4.14–4.08 (m, 1H), 3.80 (m, 2H), 3.79 (t, $J = 5.4$ Hz, 2H), 2.42 (s, 3H), 1.79–1.62 (m, 4H). ^{13}C NMR (151 MHz, CDCl_3) δ 194.95, 161.61, 161.32, 155.19, 152.51, 125.59, 113.88, 112.43, 112.14, 102.03, 67.02, 66.06, 48.74, 46.98, 35.77, 18.69. HRMS: calcd for $\text{C}_{18}\text{H}_{22}\text{NO}_4\text{S}_2$ [$\text{M} + \text{H}$] $^+$ 380.0985, found 380.1024.

4.4.7. 2-((4-methyl-2-oxo-2H-chromen-7-yl)oxy)ethyl bis(2-hydroxyethyl)carbomodithioate (4g)

Yield 82%; white solid; m.p. 100–101 °C; ^1H NMR (600 MHz, CDCl_3) δ 7.51 (d, $J = 8.4$ Hz, 1H), 6.90 (dd, $J = 8.4, 2.4$ Hz, 1H), 6.87 (d, $J = 2.4$ Hz, 1H), 6.14 (s, 1H), 4.35 (t, $J = 6.6$ Hz, 2H), 4.32 (br s, 2H), 4.16 (br s, 2H), 4.06 (br s, 2H), 3.96 (br s, 2H), 3.76 (t, $J = 6.6$ Hz, 2H), 2.40 (s, 3H). ^{13}C NMR (151 MHz, CDCl_3) δ 198.18, 161.97, 161.77, 155.43, 152.97, 125.90, 114.16, 112.94, 112.36, 102.16, 66.85, 61.00, 59.47, 58.04, 36.24, 19.00. HRMS: calcd for $\text{C}_{17}\text{H}_{22}\text{NO}_5\text{S}_2$ [$\text{M} + \text{H}$] $^+$ 384.0934, found 384.0940.

4.4.8. 2-((4-Methyl-2-oxo-2H-chromen-7-yl)oxy)ethyl 4-methylpiperazine-1-carbodi thioate (4h)

Yield 80%; white solid; m.p. 98–99 °C; ^1H NMR (600 MHz, CDCl_3) δ 7.52 (d, $J = 9.0$ Hz, 1H), 6.93 (dd, $J = 9.0, 2.4$ Hz, 1H), 6.88 (d, $J = 2.4$ Hz, 1H), 6.13 (s, 1H), 4.35 (t, $J = 6.3$ Hz, 2H), 4.23 (br s, 4H), 3.93 (br, 4H), 3.74 (t, $J = 6.5$ Hz, 2H), 2.40 (s, 3H), 1.99 (s, 3H). ^{13}C NMR (151 MHz, CDCl_3) δ 194.55, 161.46, 161.20, 155.17, 152.48, 125.64, 113.96, 112.45, 112.21, 101.88, 66.83, 53.95, 50.89, 49.58, 45.45, 35.52, 18.78. HRMS: calcd for $\text{C}_{18}\text{H}_{23}\text{N}_2\text{O}_3\text{S}_2$ [$\text{M} + \text{H}$] $^+$ 379.1145, found 379.1170.

4.4.9. 2-((4-Methyl-2-oxo-2H-chromen-7-yl)oxy)ethyl 4-isopropylpiperazine-1-carbodi thioate (4i)

Yield 88%; yellow solid; m.p. 93–94 °C; ^1H NMR (600 MHz, CDCl_3) δ 7.52 (d, $J = 8.8$ Hz, 1H), 6.93 (dd, $J = 8.8, 2.5$ Hz, 1H), 6.88 (d, $J = 2.5$ Hz, 1H), 6.16 (s, 1H), 4.40 (br s, 2H), 4.33 (t, $J = 6.3$ Hz, 2H), 4.02 (br s, 2H), 3.81 (t, $J = 6.3$ Hz, 2H), 2.81 (s, 1H), 2.66 (br s, 4H), 2.42 (s, 3H), 1.10 (s, 3H), 1.09 (s, 3H). ^{13}C NMR (151 MHz, CDCl_3) δ 195.37, 161.53, 161.26, 155.21, 152.45, 125.60, 113.89, 112.33, 112.17, 102.04, 66.97, 54.60, 51.62, 50.14, 42.97, 35.45, 18.69, 18.34. HRMS: calcd for $\text{C}_{20}\text{H}_{27}\text{N}_2\text{O}_3\text{S}_2$ [$\text{M} + \text{H}$] $^+$ 407.1458, found 407.1456.

4.4.10. 2-((4-Methyl-2-oxo-2H-chromen-7-yl)oxy)ethyl 4-cyclopropylpiperazine-1-car bodithioate (4j)

Yield 76%; yellow solid; m.p. 139–140 °C; ^1H NMR (600 MHz, CDCl_3) δ 7.52 (d, $J = 8.8$ Hz, 1H), 6.93 (dd, $J = 8.8, 2.5$ Hz, 1H), 6.88 (d, $J = 2.5$ Hz, 1H), 6.16 (s, 1H), 4.33 (t, $J = 6.7$ Hz, 2H), 4.03–3.87 (m,

4H), 3.81 (t, $J = 6.3$ Hz, 2H), 2.74 (br s, 4H), 2.41 (s, 3H), 2.06 (m, 1H), 0.50 (br s, 4H). ^{13}C NMR (151 MHz, CDCl_3) δ 195.32, 161.58, 160.97, 155.03, 152.35, 125.60, 113.89, 112.33, 112.18, 102.04, 66.90, 52.56, 39.93, 35.54, 18.65, 6.00. HRMS: calcd for $\text{C}_{20}\text{H}_{25}\text{N}_2\text{O}_4\text{S}_2$ [$\text{M} + \text{H}$] $^+$ 405.1301, found 405.1302.

4.4.11. 2-((4-Methyl-2-oxo-2H-chromen-7-yl)oxy)ethyl [1,4'-bipiperidine]-1'-carbo dithioate (4k)

Yield 89%; yellow oil; ^1H NMR (600 MHz, CDCl_3) δ 7.54 (d, $J = 9.0$ Hz, 1H), 6.95 (dd, $J = 9.0$ Hz, $J = 2.4$ Hz, 1H), 6.89 (d, $J = 2.4$ Hz, 1H), 6.17 (s, 1H), 4.34 (t, $J = 6.6$ Hz, 2H), 3.82 (br s, 2H), 3.25 (br s, 3H), 2.70 (br s, 1H), 2.57 (br s, 4H), 2.43 (s, 3H), 2.00 (br s, 3H), 1.65 (br s, 6H), 1.49 (br s, 2H). ^{13}C NMR (151 MHz, CDCl_3) δ 194.86, 161.56, 161.30, 155.20, 152.49, 125.60, 113.87, 112.35, 112.15, 102.04, 67.01, 61.97, 60.63, 50.28, 35.69, 29.71, 26.11, 25.66, 24.53, 22.09, 18.69. HRMS: calcd for $\text{C}_{23}\text{H}_{31}\text{N}_2\text{O}_3\text{S}_2$ [$\text{M} + \text{H}$] $^+$ 447.1771, found 447.1766.

4.4.12. 2-((4-Methyl-2-oxo-2H-chromen-7-yl)oxy)ethyl 4-(pyrimidin-2-yl)piperazine- 1-carbodithioate (4l)

Yield 86%; white solid; m.p. 195–196 °C; ^1H NMR (600 MHz, CDCl_3) δ 8.47 (d, $J = 4.8$ Hz, 2H), 7.53 (d, $J = 8.4$ Hz, 1H), 6.94 (dd, $J = 8.4, 2.4$ Hz, 1H), 6.88 (d, $J = 2.4$ Hz, 1H), 6.73 (t, $J = 4.8$ Hz, 1H), 6.16 (s, 1H), 4.48 (br s, 4H), 4.35 (t, $J = 6.6$ Hz, 2H), 4.11 (br s, 4H), 3.84 (t, $J = 6.6$ Hz, 2H), 2.42 (s, 3H). ^{13}C NMR (151 MHz, CDCl_3) δ 196.26, 161.50, 161.24, 157.83, 155.21, 152.43, 125.60, 113.91, 112.33, 112.19, 110.76, 102.01, 68.86, 42.97, 38.73, 35.50, 29.80, 28.93, 18.68. HRMS: calcd for $\text{C}_{21}\text{H}_{23}\text{N}_4\text{O}_3\text{S}_2$ [$\text{M} + \text{H}$] $^+$ 443.1206, found 443.1153.

4.4.13. 3-((4-Methyl-2-oxo-2H-chromen-7-yl)oxy)propyl piperidine-1-carbodithioate (4m)

Yield 89%; white solid; m.p. 87–88 °C; ^1H NMR (600 MHz, CDCl_3) δ 7.54 (d, $J = 9.0$ Hz, 1H), 6.90 (dd, $J = 9.0, 2.4$ Hz, 1H), 6.86 (d, $J = 2.4$ Hz, 1H), 6.17 (s, 1H), 4.32 (br s, 2H), 4.16 (t, $J = 6.0$ Hz, 2H), 3.92 (br s, 2H), 3.54 (t, $J = 6.6$ Hz, 2H), 2.42 (s, 3H), 2.30–2.26 (m, 2H), 1.76–1.69 (br s, 6H). ^{13}C NMR (151 MHz, CDCl_3) δ 195.12, 161.93, 155.29, 152.48, 125.61, 113.82, 112.44, 111.97, 101.60, 67.95, 53.10, 51.27, 38.68, 28.90, 24.26, 23.00, 18.59. HRMS: calcd for $\text{C}_{19}\text{H}_{24}\text{NO}_3\text{S}_2$ [$\text{M} + \text{H}$] $^+$ 378.1187, found 378.1209.

4.4.14. 4-((4-Methyl-2-oxo-2H-chromen-7-yl)oxy)butyl piperidine- 1-carbodithioate (4n)

Yield 83%; white solid; m.p. 91–92 °C; ^1H NMR (600 MHz, CDCl_3) δ 7.49 (d, $J = 9.0$ Hz, 1H), 6.87 (dd, $J = 9.0, 2.4$ Hz, 1H), 6.81 (d, $J = 2.4$ Hz, 1H), 6.13 (s, 1H), 4.30 (br s, 2H), 4.06 (t, $J = 6.6$ Hz, 2H), 3.90 (br s, 2H), 3.40 (t, $J = 7.2$ Hz, 2H), 2.40 (s, 3H), 1.97–1.92 (m, 4H), 1.72–1.69 (m, 6H). ^{13}C NMR (151 MHz, CDCl_3) δ 195.55, 162.06, 161.37, 155.29, 152.57, 125.50, 113.52, 112.64, 111.90, 101.43, 67.99, 52.97, 51.27, 36.63, 28.24, 25.56, 24.33, 18.69. HRMS: calcd for $\text{C}_{20}\text{H}_{26}\text{NO}_3\text{S}_2$ [$\text{M} + \text{H}$] $^+$ 392.1349, found 392.1346.

4.4.15. 5-((4-Methyl-2-oxo-2H-chromen-7-yl)oxy)pentyl piperidine-1-carbodithioate (4o)

Yield 80%; white solid; m.p. 88–89 °C; ^1H NMR (600 MHz, CDCl_3) δ 7.51 (d, $J = 8.8$ Hz, 1H), 6.87 (dd, $J = 8.8, 2.5$ Hz, 1H), 6.82 (d, $J = 2.5$ Hz, 1H), 6.15 (s, 1H), 4.32 (s, 2H), 4.05 (t, $J = 6.4$ Hz, 2H), 3.92 (br s, 2H), 3.36 (t, $J = 6.4$ Hz, 2H), 2.42 (s, 3H), 1.92–1.86 (m, 2H), 1.84–1.79 (m, 2H), 1.77–1.58 (m, 8H). ^{13}C NMR (151 MHz, CDCl_3) δ 195.80, 162.16, 161.39, 155.31, 152.59, 125.50, 113.47, 112.64, 111.87, 101.41, 68.31, 52.79, 51.32, 36.91, 28.57, 28.56, 25.40, 24.34, 18.69. HRMS: calcd for $\text{C}_{21}\text{H}_{28}\text{NO}_3\text{S}_2$ [$\text{M} + \text{H}$] $^+$ 406.1505, found 406.1491.

4.4.16. 6-((4-Methyl-2-oxo-2H-chromen-7-yl)oxy)hexyl piperidine-1-carbodithioate (4p)

Yield 87%; white solid; m.p. 64–65 °C; ^1H NMR (600 MHz, CDCl_3) δ 7.50 (d, $J = 9.0$ Hz, 1H), 6.86 (dd, $J = 8.8, 2.4$ Hz, 1H), 6.80 (d,

$J = 2.4$ Hz, 1H), 6.13 (s, 1H), 4.30 (br s, 2H), 4.03 (t, $J = 6.6$ Hz, 2H), 3.90 (br s, 2H), 3.32 (t, $J = 7.2$ Hz, 2H), 2.40 (s, 3H), 1.85–1.81 (m, 2H), 1.77–1.68 (m, 8H), 1.53–1.51 (m, 4H). ^{13}C NMR (151 MHz, CDCl_3) δ 196.31, 162.56, 161.75, 155.68, 152.95, 125.84, 113.80, 113.05, 112.20, 101.73, 68.81, 53.18, 51.59, 37.42, 29.21, 29.04, 29.03, 25.95, 24.71, 19.05. HRMS: calcd for $\text{C}_{22}\text{H}_{30}\text{NO}_3\text{S}_2$ [$\text{M} + \text{H}$] $^+$ 420.1662, found 420.1638.

4.4.17. 8-((4-Methyl-2-oxo-2H-chromen-7-yl)oxy)octyl piperidine-1-carbodithioate (**4q**)

Yield 86%; white solid; m.p. 60–61 °C; ^1H NMR (600 MHz, CDCl_3) δ 7.51 (d, $J = 8.8$ Hz, 1H), 6.87 (dd, $J = 8.8, 2.5$ Hz, 1H), 6.83 (d, $J = 2.5$ Hz, 1H), 6.15 (s, 1H), 4.32 (br s, 2H), 4.03 (t, $J = 6.5$ Hz, 2H), 3.91 (br s, 2H), 3.35–3.29 (m, 2H), 2.42 (s, 3H), 1.87–1.80 (m, 2H), 1.75–1.72 (m, 2H), 1.54–1.25 (m, 14H). ^{13}C NMR (151 MHz, CDCl_3) δ 196.09, 162.25, 161.42, 155.33, 152.60, 125.47, 113.42, 112.71, 111.85, 101.37, 68.55, 52.74, 51.22, 37.24, 30.37, 29.16, 29.07, 28.96, 28.93, 28.68, 25.89, 24.35, 23.75, 18.69. HRMS: calcd for $\text{C}_{24}\text{H}_{34}\text{NO}_3\text{S}_2$ [$\text{M} + \text{H}$] $^+$ 448.1975, found 448.1901.

5. Biological evaluation

5.1. Inhibition experiments of ChEs

Acetylcholinesterase (AChE, E.C. 3.1.1.7) from human erythrocytes, butylcholinesterase (BuChE, E.C. 3.1.1.8) from human serum, S-butylthiocholine iodide (BTCl), acetylthiocholine iodide (ATCl), 5, 5'-dithiobis-(2-nitrobenzoic acid) (Ellman's reagent, DTNB), donepezil hydrochloride was purchased from Sigma-Aldrich (St. Louis, MO, USA). The inhibitory activities of test compounds **4a–q** were evaluated by Ellman's method [33]. The compounds were dissolved in DMSO and diluted with the buffer solution (50 mM Tris-HCl, pH = 8.0, 0.1 M NaCl, 0.02 M $\text{MgCl}_2 \cdot 6\text{H}_2\text{O}$) to yield corresponding test concentrations (DMSO less than 0.01%). In each well of the plate, 160 μL of 1.5 mM DTNB, 50 μL of AChE (0.05 U/mL hAChE) or 50 μL of BuChE (0.024 U/mL hBuChE) were incubated with 10 μL of different concentrations of test compounds at 37 °C for 6 min. After this period, acetylthiocholine iodide (15 mM) or S-butylthiocholine iodide (15 mM) as the substrate (30 μL) was added and the absorbance was measured with a wavelength of 405 nm at different time intervals (0, 60, 120, and 180 s). IC_{50} values were calculated as concentration of compound that produces 50% enzyme activity inhibition, using the Graph Pad Prism 4.03 software (San Diego, CA, USA). Results are expressed as the mean \pm SD of at least three different experiments performed in triplicate.

5.2. Kinetic study of AChE inhibition

The kinetic study of AChE was performed by Ellman's method with three different concentrations (12.5, 25 and 50 nM) of compound **4n**. Lineweaver–Burk reciprocal plots were constructed by plotting $1/\text{velocity}$ against $1/[\text{substrate}]$ at varying concentrations of the substrate acetylthiocholine (0.05–0.50 mM). The plots were assessed by a weighted least-squares analysis that assumed the variance of velocity (v) to be a constant percentage of v for the entire data set. Data analysis was performed with Graph Pad Prism 4.03 software (San Diego, CA, USA).

5.3. Molecular modeling studies

Molecular modeling calculations and docking studies were performed using Molecular Operating Environment (MOE) software version 2008.10 (Chemical Computing Group, Montreal, Canada). The X-ray crystallographic structure of AChE (PDB code 4EY7) was obtained from the Protein Data Bank. All water

molecules in PDB files were removed and hydrogen atoms were subsequently added to the protein. The compound **4n** was constructed using the MOE builder module and energy minimized using Merck Molecular force field (MMFF94x, RMSD gradient: $0.05 \text{ kcal mol}^{-1} \text{ \AA}^{-1}$). The protonation level of the compound in physiological pH was calculated by the Marvin 14.12.8 2014 software package, ChemAxon [<http://www.chemaxon.com>]. Then the **4n** was docked into the active site of the protein by the “Triangle Matcher” method, which generated poses by aligning the ligand triplet of atoms with the triplet of alpha spheres in cavities of tight atomic packing. The Dock scoring in MOE software was done using ASE scoring function and Force field was selected as the refinement method. The best 10 poses of molecules were retained and scored. After docking, the geometry of resulting complex was studied using the MOE's pose viewer utility.

5.4. Inhibition of $\text{A}\beta_{1-42}$ self-induced aggregation

Inhibition of self-induced $\text{A}\beta_{1-42}$ aggregation was measured using a Thioflavin T (ThT)-binding assay [37]. HFIP pretreated $\text{A}\beta_{1-42}$ samples (Anaspec Inc) were resolubilized with a 50 mM phosphate buffer (pH 7.4) to give a 25 μM solution. Each tested compound was firstly prepared in dimethyl sulfoxide (DMSO) and 1 μL of each was added to the well of black, opaque Corning 96-well plates such that the final solvent concentration was 10%. The final concentration of each compound was 25 μM and was prepared in independent triplicates. The solvent control was also included. Then, 9 μL of 25 mM $\text{A}\beta_{1-42}$ sample was added to each well and the samples mixed by gentle trapping. Plates were covered to minimize evaporation and incubated in dark at room temperature for 46–48 h with no agitation.

After the incubation period, 200 μL of 5 μM ThT in 50 mM glycine-NaOH buffer (pH 8.0) was added to each well. Fluorescence was measured on a SpectraMax M5 (Molecular Devices, Sunnyvale, CA, USA) multi-mode plate reader with excitation and emission wavelengths at 446 nm and 490 nm, respectively. The fluorescence intensities were compared and the percent inhibition due to the presence of the inhibitor was calculated by the following formula: $100 - (\text{IF}_i/\text{IF}_0 \times 100)$ where IF_i and IF_0 are the fluorescence intensities obtained for $\text{A}\beta_{1-42}$ in the presence and in the absence of inhibitor, respectively.

5.5. Metal-chelating studies

The metal-chelating ability of compound **4n** were studied using a UV–vis spectrophotometer at wavelength ranging from 200 to 500 nm [38]. The UV absorption of compound, alone or in the presence of CuCl_2 , ZnCl_2 , FeSO_4 and $\text{Fe}_2(\text{SO}_4)_3$, were recorded after incubating for 30 min in menthol at room temperature. The final volume of reaction mixture was 3 mL. The final concentrations of compound **4n** and metals were 25 μM and 50 μM , respectively.

The stoichiometry of the **4n**- Fe^{3+} complex was determined by Job's method [39]. The method is that keeping the total concentration of compound and Fe^{3+} at 50 μM , and varying the molar ratio of Fe^{3+} from 0.1 to 0.9. The absorbance change at 373 nm were plotted versus the mole fraction, showing a maximum at 0.5, which revealed a stoichiometry of 1:1 for **4n**- Fe^{3+} complex. The association constant (K_a) was calculated by the Benesi-Hildebrand equation as follows [39,40]: $1/A - A_0 = 1/K_a (A_{\text{max}} - A_0) [\text{Fe}^{3+}] + 1/A_{\text{max}} - A_0$, where A and A_0 represent the absorbance of compound in the presence and absence of Fe^{3+} , respectively. A_{max} is the saturated absorbance of the compound in the presence of excess amount of $[\text{Fe}^{3+}]$; $[\text{Fe}^{3+}]$ is the concentration of Fe^{3+} ion added.

5.6. SH-SY5Y neuroblastoma cell toxicity

The cytotoxicity effect of test compound on the human neuroblastoma SH-SY5Y cells was evaluated by MTT assay according to a described method [41]. The SH-SY5Y cells were grown in a 1:1 mixture of Eagle's minimum essential medium (EMEM) and ham's F-12 medium supplemented with 10% fetal bovine serum (FBS), 100 U/mL penicillin and 100 µg/mL streptomycin in 5% CO₂ at 37 °C. For cell viability assay, cells were placed into 96-well plates at a seeding density of 10000 cells/well and incubated with compound **4n** for 24 h. After this incubation, 20 µL of MTT at 37 °C was added for 4 h. Then, the medium was removed, and 200 µL of DMSO was added to dissolve the formazan crystal formed. The absorbance was measured in a microculture plate reader with a test wavelength of 570 nm and a reference wavelength of 630 nm. Results are expressed as the mean ± SD of three independent experiments.

5.7. In vitro blood-brain barrier permeation assay

The ability of test compounds that penetrate into brain was evaluated using a parallel artificial membrane permeation assay (PAMPA) for blood-brain-barrier according to the method established by Di et al. [42]. Commercial drugs, PBS (pH = 7.4), DMSO and dodecane were obtained from Sigma and Aladdin. Porcine brain lipid (PBL) was purchased from Avanti Polar Lipids. The donor microplate (96-well filter plate, PVDF membrane, pore size is 0.45 µm) and the acceptor microplate (indented 96-well plate) were both from Millipore. The 96-well UV plate (COSTAR) was acquired from Corning Inc. The compound was firstly dissolved in DMSO at a concentration of 5 mg/mL. Then, it was diluted 200-fold with a mixture of PBS/EtOH (70:30) to give a final concentration of 25 µg/mL. The filter membrane in donor microplate was coated with PBL dissolved in dodecane (4 µL, 20 mg/mL). After that, 200 µL of diluted solution and 300 µL of PBS/EtOH (70:30) were added to the donor wells and the acceptor wells, respectively. The donor filter plate was carefully placed on the acceptor plate to make the underside of filter membrane can contact with buffer solution. After leaving this sandwich assembly undisturbedly for 16 h at 25 °C, the donor plate was carefully removed, and the concentrations of test compound in the acceptor, donor and reference wells were measured with a UV plate reader (SpectraMax Plus 384, Molecular Devices, Sunnyvale, CA, USA). Each sample was analyzed at least three independent runs in four wells, and the results are given as the means ± SD. P_e was calculated using the following expression: $P_e = \{-V_d V_a / [(V_d + V_a) A t] \ln(1 - \text{drug}_{\text{acceptor}} / \text{drug}_{\text{equilibrium}})\}$, where V_d is the volume of donor well, V_a is the volume in the acceptor well, A is the filter area, t is the permeation time, drug acceptor is the absorbance obtained in the acceptor well, and drug equilibrium is the theoretical equilibrium absorbance. A plot of the experimental P_e values of 10 standard drugs versus their bibliographic values provided a good linear correlation, $P_e(\text{exp.}) = 1.2653 P_e(\text{bibl.}) + 0.7955$ ($R^2 = 0.9483$).

5.8. Acute toxicity test [43,44]

Twenty-four Kunming mice (20 ± 2 g) were supplied by Hunan SJA Laboratory Animal Co., Ltd (eligibility certification no. SCXK [xiang] 2016–0004). Animals were housed in stainless steel cages by sex in a ventilated animal room and maintained under standard conditions with a 12 h:12 h light/dark cycle. Distilled water and sterilized food for mice were available ad libitum. They were acclimated to this environment for 5 days prior to dosing.

Animals were randomly divided into two groups: control group and experimental group (1000 mg/kg, $n = 12$ per group). Before treatment, animals were fasted overnight. Compound **4n** was

suspended in 0.5% carboxymethyl cellulose sodium (CMC-Na) salt solution and orally administered according to the divided groups. Food and water were provided later. After administration of **4n**, the mice were observed continuously for the first 4 h for any abnormal behavior and mortality changes, intermittently for the next 24 h, and occasionally thereafter for 14 days for the onset of any delayed effects. All animals were sacrificed after being anaesthetized by ether on the 14th day after drug administration.

5.9. Step-down passive avoidance test

Donepezil hydrochloride was purchased from the Energy Chemical Co., Ltd (Shanghai, China). Scopolamine was obtained from Suicheng Pharmaceutical Co. Ltd. (Zhengzhou, China). Male Kunming mice weighting 18–22 g were supplied by Hunan SJA Laboratory Animal Co., Ltd (eligibility certification no. SCXK [xiang] 2017–0002). Animals were maintained in our animal house controlled at constant temperature of 23 ± 2 °C with a relative humidity of 55 ± 5% and a 12 h light/dark cycle. They were allowed free access to tap water and standard laboratory chow.

The step-down test was carried in the passive avoidance chamber with a steel grid floor [45]. A plastic platform was placed in bottom right corner of the chamber. Illumination was available in the light box through LED lights at 250 lx. The mice underwent two separate trials: a training trial and a recall trial. For the training trial, each mouse was allowed to get familiar with the chamber for 5 min. Then the power was on and the mouse was placed on the platform. Once the mouse stepped down, it would receive an electric shock (24 V, 0.5 mA), which caused it to return to the platform. We used a total of 48 mice in the passive avoidance test with 8 mice were used per treatment. Compounds **4n** (20.6, 10.3 and 5.2 mg/kg, p.o.) or donepezil (5.0 mg/kg, p.o.) as a positive control were orally given 1 h before each training trial. After 30 min, memory impairment was induced by administering scopolamine (3 mg/kg, i.p.). After a 24 h interval, the recall trial was performed, and the mice were placed on the platform again. The latency to step down on the grid for the first time and the errors that resulted in a shock within 5 min were measured as the learning and memory performance.

Acknowledgement

This research work was financially supported by the Program of the National Natural Science Foundation of China [Grant No. 81760622, 31600265]; the Program of Natural Science Foundation of Guangxi Province of China [grant No. 2017GXNSFAA198077]; the Program of Natural Science Foundation of Jiangxi Province of China [grant No. 20171BAB215064]; Research Fund for the Doctoral Program of Jiangxi University of Traditional Chinese Medicine [Grant No. 2015BS008]; the Program of Basic ability enhancement of young teachers in Guangxi colleges and universities [Grant No. KY2016YB091]; Guangxi Key Laboratory of Brain and Cognitive Neuroscience, Guilin Medical University [07010150001]; Project from Health and Family planning Commission of Jiangxi province [Grant No. 2016A048, 20173013].

Appendix A. Supplementary data

Supplementary data associated with this article can be found in the online version, at <https://doi.org/10.1016/j.ejmech.2018.01.055>. These data include MOL files and InChIKeys of the most important compounds described in this article.

References

- [1] M. Goedert, M.G. Spillantini, *Sci. (New York, N.Y.)* 314 (2006) 777–781.

- [2] S. Salloway, J. Mintzer, M.F. Weiner, J.L. Cummings, *Alzheimers Dement* 4 (2008) 65–79.
- [3] H. Tang, H.T. Zhao, S.M. Zhong, Z.Y. Wang, Z.F. Chen, H. Liang, *Bioorg. Med. Chem. Lett* 22 (2012) 2257–2261.
- [4] E. Scarpini, P. Schelterns, H. Feldman, *Lancet Neurol.* 2 (2003) 539–547.
- [5] N. Herrmann, S.A. Chau, I. Kircanski, K.L. Lancôt, *Drugs* 71 (2011) 2031–2065.
- [6] J. Godyń, J. Jończyk, D. Panek, B. Malawska, *Pharmacol. Rep.* 68 (2016) 127–138.
- [7] R.T. Bartus, R.L. Dean, B. Beer, A.S. Lipka, *Science* 217 (1982) 408–417.
- [8] B.Z. Kurt, I. Gazioglu, L. Basile, F. Sonmez, T. Ginex, M. Kucukislamoglu, S. Guccione, *Eur. J. Med. Chem.* 102 (2015) 80–92.
- [9] A. Romero, R. Cacabelos, M.J. Oset-Gasque, A. Samadi, J. Marco-Contelles, *Bioorg. Med. Chem. Lett* 23 (2013) 1916–1922.
- [10] J.L. Sussman, M. Harel, F. Frolow, C. Oefner, A. Goldman, L. Toker, I. Silman, *Science* 253 (1991) 872–879.
- [11] Y. Chen, J. Sun, L. Fang, M. Liu, S. Peng, H. Liao, J. Lehmann, Y. Zhang, *J. Med. Chem.* 55 (2012) 4309–4321.
- [12] R. Leurs, R.A. Bakker, H. Timmerman, I. de Esch, *J. Nat. Rev. Drug Discov.* 4 (2005) 107–120.
- [13] I. Peretto, S. Radaelli, C. Parini, M. Zandi, L.F. Raveglia, G. Dondio, L. Fontanella, P. Misiano, C. Bigogno, A. Rizzi, B. Riccardi, M. Biscaioli, S. Marchetti, P. Puccini, S. Catinella, I. Rondelli, V. Cenacchi, P.T. Bolzoni, P. Caruso, G. Villetti, F. Facchinetti, E. Del Giudice, N. Moretto, B.P. Imbimbo, *J. Med. Chem.* 48 (2005) 5705–5720.
- [14] Y. Li, X. Qiang, L. Luo, X. Yang, G. Xiao, Q. Liu, J. Ai, Z. Tan, Y. Deng, *Eur. J. Med. Chem.* 126 (2017) 762–775.
- [15] J. Hardy, D.J. Selkoe, *Science* 297 (2002) 353–356.
- [16] A.K. Sharma, S.T. Pavlova, J. Kim, D. Finkelstein, N.J. Hawco, N.P. Rath, J. Kim, L.M. Mirica, *J. Am. Chem. Soc.* 134 (2012) 6625–6636.
- [17] N. Jiang, X.B. Wang, Z.R. Li, S.Y. Li, S.S. Xie, M. Huang, L.Y. Kong, *RSC Adv.* 5 (2015) 14242–14255.
- [18] R. León, A.G. Garcia, J. Marco-Contelles, *Med. Res. Rev.* 33 (2013) 139–189.
- [19] G. Pepeu, M.G. Giovannini, *Curr. Alzheimer Res.* 6 (2009) 86–96.
- [20] J. Dong, C.S. Atwood, V.E. Anderson, S.L. Siedlak, M.A. Smith, G. Perry, P.R. Carey, *Biochemistry* 42 (2003) 2768–2773.
- [21] F. Gu, M. Zhu, J. Shi, Y. Hu, Z. Zhao, *Neurosci. Lett.* 440 (2008) 44–48.
- [22] D.A. Butterfield, A.M. Swomley, R. Sultana, *Antioxidants Redox Signal.* 19 (2013) 823–835.
- [23] N. Jiang, S.Y. Li, S.S. Xie, Z.R. Li, K.D. Wang, X.B. Wang, L.Y. Kong, *Eur. J. Med. Chem.* 87 (2014) 540–551.
- [24] S.S. Xie, X. Wang, N. Jiang, W. Yu, K.D. Wang, J.S. Lan, Z.R. Li, L.Y. Kong, *Eur. J. Med. Chem.* 95 (2015) 153–165.
- [25] I. Kostova, S. Bhatia, P. Grigorov, S. Balkansky, V.S. Parmar, A.K. Prasad, L. Saso, *Curr. Med. Chem.* 18 (2011) 3929–3951.
- [26] P. Anand, B. Singh, N. Singh, *Bioorg. Med. Chem.* 20 (2012) 1175–1180.
- [27] J.B. Shaik, B.K. Palaka, M. Penumala, K.V. Kotapati, S.R. Devineni, S. Eadlapalli, M.M. Darla, D.R. Ampasala, R. Vadde, G.D. Amooru, *Eur. J. Med. Chem.* 107 (2016) 219–232.
- [28] J.B. Shaik, B.K. Palaka, M. Penumala, S. Eadlapalli, M.D. Mark, D.R. Ampasala, R. Vadde, D.A. Gangaiah, *Chem. Biol. Drug Des.* 88 (2016) 43–53.
- [29] J.S. Lan, Y. Ding, Y. Liu, P. Kang, J.W. Hou, X.Y. Zhang, S.S. Xie, T. Zhang, *Eur. J. Med. Chem.* 139 (2017) 48–59.
- [30] Y.C. Duan, Y.C. Ma, E. Zhang, X.J. Shi, M.M. Wang, X.W. Ye, H.M. Liu, *Eur. J. Med. Chem.* 62 (2013) 11–19.
- [31] S.S. Xie, X.B. Wang, J.Y. Li, L. Yang, L.Y. Kong, *Eur. J. Med. Chem.* 64 (2013), 540–533.
- [32] R.D. Li, H.L. Wang, Y.B. Li, Z.Q. Wang, X. Wang, Y.T. Wang, Z.M. Ge, R.T. Li, *Eur. J. Med. Chem.* 93 (2015) 381–391.
- [33] G.L. Ellman, K.D. Courtney, V. Andres Jr., R.M. Feather-Stone, *Biochem. Pharmacol.* 7 (1961) 88–95.
- [34] M.D. Altintop, A.S. Gurkan-Alp, Y. Ozkay, Z.A. Kaplancikli, *Arch. Pharm.* 346 (2013) 571–578.
- [35] U.A. Mohsen, Z.A. Kaplancikli, Y. Ozkay, L. Yurttas, *Drug Res.* 65 (2015) 176–183.
- [36] M. Rosini, E. Simoni, M. Bartolini, A. Cavalli, L. Ceccarini, N. Pascu, D.W. McClymont, A. Tarozzi, M.L. Bolognesi, A. Minarini, V. Tumiatti, V. Andrisano, I.R. Mellor, C. Melchiorre, *J. Med. Chem.* 51 (2008) 4381–4384.
- [37] M. Bartolini, C. Bertucci, M.L. Bolognesi, A. Cavalli, C. Melchiorre, V. Andrisano, *ChemBiochem* 8 (2007) 2152–2161.
- [38] M. I. Fernandez-Bachiller, C. Perez, G. C. Gonzalez-Munoz, S. Conde, M. G. Lopez, M. Villarroya, A. G. Garcia, M. I. Rodriguez-Franco, *J. Med. Chem.* 53 (2010) 4927–4937.
- [39] L.Y. Wang, D.C. Ye, D.R. Cao, *Spectrochim. Acta, Part A* 90 (2012) 40–41.
- [40] H.A. Benesi, J.H. Hildebrand, *J. Am. Chem. Soc.* 71 (1949) 2703–2707.
- [41] X. Li, H. Wang, Z. Lu, X. Zheng, W. Ni, J. Zhu, Y. Fu, F. Lian, N. Zhang, J. Li, H. Zhang, F. Mao, *J. Med. Chem.* 59 (2016) 8326–8344.
- [42] L. Di, E.H. Kerns, K. Fan, O.J. McConnell, G.T. Carter, *Eur. J. Med. Chem.* 38 (2003) 223–232.
- [43] C. Lu, Y. Guo, J. Yan, Z. Luo, H.B. Luo, M. Yan, L. Huang, X. Li, *J. Med. Chem.* 56 (2013) 5843–5859.
- [44] J.S. Lan, T. Zhang, Y. Liu, J. Yang, S.S. Xie, J. Liu, Z.Y. Miao, Y. Ding, *Eur. J. Med. Chem.* 133 (2017) 184–196.
- [45] I. Klivenberg, A. Blokland, *Neurosci. Biobehav. Rev.* 34 (2010) 1307–1350.
- [46] Z. Sang, W. Pan, K. Wang, Q. Ma, L. Yu, Y. Yang, P. Bai, C. Leng, Q. Xu, X. Li, Z. Tan, W. Liu, *Eur. J. Med. Chem.* 130 (2017) 379–392.